ESA Climate Change Initiative
River Discharge Precursor (RD_cci+)

D.3 River Discharge (RD) from altimeters, river-width, multispectral images and data combination Algorithm Theoretical Basis Document (ATBD)

Contract number: 4000139952/22/I-NB

Reference: RD_CCI-0006-ATBD

Issue 2.0 – 31/07/2025

11 rue Hermès, Parc Technologique du Canal — 31520 Ramonville Saint-Agne, France
Tel +33 (0)5 61 39 47 00 Fax +33(0)5 61 75 10 14
www.cls.fr

CHRONOLOGY ISSUES

Issue	Date	Object	Written by
1.0	18/12/23	Initial version	Laetitia Gal and Angelica Tarpanelli
1.1	12/01/24	New version replying to ESA comments	Laetitia Gal and Angelica Tarpanelli
1.2	26/09/24	Updated version with last RD-multispec and RD-merged products	Laetitia Gal and Angelica Tarpanelli
2.0	31/07/25	Updated version with river-width based RD, complement on RD-alti, RD-multispec and RD-merged	Laetitia Gal, Angelica Tarpanelli, Mohammad Tourian, and Paolo Filippucci

Checked by	S. Biancamaria - LEGOS	sylvain.biancamaria 22/09/2025
Approved by	Philippe Mourot - CLS	Pmourot 24/09/2025
Authorized by	Clément Albergel - ESA	clement.albergel 01/10/2025

DISTRIBUTION

Company	Names	Email
ESA	Clément Albergel	clement.albergel@esa.int
CLS	Philippe Mourot	pmourot@groupcls.com
CLS	Daya Ceccone	dceccone@groupcls.com
CLS	Maxime Vayre	mvayre@groupcls.com
CLS	Nicolas Taburet	ntaburet@groupcls.com
CLS	Gabriel Calassou	gcalassou@groupcls.com
CNRM	Simon Munier	simon.munier@meteo.fr
EOLA	Elena Zakharova	zavocado@gmail.com
Hydromatters	Malik Boussaroque	malik.boussaroque@hydro-matters.fr
Hydromatters	Laetitia Gal	laetitia.gal@hydro-matters.fr
Hydromatters	Adrien Paris	adrien.paris@hydro-matters.fr
IRPI	Silvia Barbetta	silvia.barbetta@irpi.cnr.it
IRPI	Angelica Tarpanelli	angelica.tarpanelli@irpi.cnr.it
IRPI	Paolo Filippucci	paolo.filippucci@irpi.cnr.it
LEGOS-CNRS	Sylvain Biancamaria	sylvain.biancamaria@univ-tlse3.fr
LEGOS-CNES	Julien Lefebve	julien.lefebve@cnes.fr
LEGOS	Benjamin Kitambo	benjamin.kitambo@univ-tlse3.fr
GEOS-IRD	Fabrice Papa	fabrice.papa@ird.fr
Magellium	Gilles Larnicol	gilles.larnicol@magellium.fr
Magellium	Vanessa Pedinotti	vanessa.pedinotti@magellium.fr
Magellium	Malak Sadki	malak.sadki@magellium.fr
Univ. Stuttgart	Mohammad Tourian	tourian@gis.uni-stuttgart.de
LEGOS-IRD	Nino Fernando	fernando.nino@ird.fr
LEGOS	Fabien Blarel	fabien.blarel@univ-tlse3.fr
PML	Stefan Simis	stsi@pml.ac.uk
Univ. Exeter - PML	Jareno Nuria Bachiller	nb748@exeter.ac.uk

LIST OF CONTENTS/SOMMAIRE

1 Introduction 7
2 Available ancillary data 7
3 Calibration – Validation periods 10
4 Derive discharge from altimeters (RD-alti) 12
4.1 Context 12
4.2 Bayesian-based Rating Curve (RC) estimation 13
4.2.1 Bayesian approach 13
4.2.2 WSE data type 15
4.2.3 Method 1 – Bayesian estimation using overlapping dataset – preferred approach 16
4.2.4 Method 2 – Bayesian estimation using quantile-based matching – alternative approach 18
4.3 Uncertainties 19
5 Derive discharge from river-width (RD-width) 20
5.1 River width estimation using optical satellite imagery 20
5.2 River discharge estimation using river width 21
6 Derive discharge from multispectral images (RD-multispec) 23
6.1 Context 23
6.2 Reflectance indices definition 23
6.3 Multi-mission reflectance time series 24
6.4 River discharge estimation from reflectance indices 27
6.4.1 Calibrated Approach 27
6.4.2 Uncalibrated Approach 28
7 Derive discharge from merged products 29
8 References 29

LIST OF TABLES AND FIGURES

Figure 1: Available discharge data for all stations from different sources 9
Figure 2: Available data for in situ discharge from various sources (blue) and merged water surface elevation from altimeter (green) from each station. The period where the two data sets overlap is represented in red with the number of overlap's days. 10
Figure 3: Rating curve computation methodology 13
Figure 4: Rating curve for the Near-Brookings station (Mississippi basin) before (left) and after (right) excluding data points associated with temperature variations (below 0°C). 17
Figure 5: Flowchart of the stochastic quantile mapping function algorithm (adapted from Elmi et at., 2021, and Saemian et al., 2024) 22
Figure 6: Weights of the daily data of each sensor according to the temporal distance by the nearest sensing day. The weights are distributed with a gaussian function River. 27

Table 1: Summary of the calibration and validation periods for each station, along with the number of days available for both calibration and validation. Stations marked with an asterisk (*) indicate cases where there is too little overlap between discharge and water surface elevation data to separate into calibration and validation periods. In these instances, all available data will be used for calibration or another method to derive discharge from altimetry will be use. 11
Table 2: Description of the datasets for multispectral images. It includes selected product, reflectance type, platform used to analyze the data (GEE is Google Earth Engine, SH is Sentinel-HUB, EC is Earth Console), period of data availability, spatial resolution and revisit time. 25

REFERENCE DOCUMENTS

[**RD-1**] D.2. Selection of river basins. CCI River Discharge precursor project Document (CCI-Discharge-0004-RP_WP2, Issue 1.0)

[**RD-2**] D.3.1. Water Surface Elevation (WSE) Algorithm Theoretical Basis Document (ATBD) (CCI-Discharge-0005-ATBD-WSE, Issue 2.0)

[**RD-3**] he ESA river discharge CCI project - https://climate.esa.int/en/projects/river-discharge/about-the-river-discharge-project/

LIST OF ACRONYMS

AIPo	Agenzia Interregionale del Fiume Po
ArcticGRO	The Arctic Great Rivers Observatory
ATBD	Algorithm Theoretical Basis Document
CCI	Climate Change Initiative
CDF	Cumulative Distribution Function
eDT	ending datetime
EO	Earth Observation
FABDEM	Forest And Buildings removed Copernicus DEM
GRDC	Global Runoff Data Centre
GSW	Global Surface Water
MCMC	Markov Chain Monte Carlo
NPQM	Non-Parametric Quantile Mapping
Q	Discharge
RC	Rating Curve
RD	River Discharge
RD-alti	Altimetry-based River Discharge
RD-multispec	Multispectral images-based River Discharge
RD-merge	Satellite-based River Discharge – merging approach
RD-mergeL2	RD-merge – merging approach using Level 2 products (WSE/CM)
RD-mergeL3	RD-merge – merging approach using Level 3 products (RD-alti/RD-multispec)
RD-width	Width-based River Discharge
RivDIS	The Global River Discharge
RMSE	Root Mean Squared Error
SCHAPI	Service Central d'Hydrométéorologie et d'Appui à la Prévision des Inondations
sDT	starting datetime
SO-HYBAM	Service d'Observation - HYdro-géochimie du Bassin AMazonien
SWORD	SWOT River Database
USGS	The U.S. Geological Survey's
WP	Work Package
WSE	Water Surface Elevation

1 Introduction

This document provides an overview of the theoretical framework underlying the algorithm employed in computing long discharge time series data (Q) using different approaches.

Section two of this document will focus on discussing the available ancillary data essential for implementing these two approaches. Following that, the third section will delve into defining calibration and validation periods for each station as defined in [RD-1] and updated when WSE time series have been computed [RD-2].

Subsequently, section four will elaborate on the methodology used to derive discharge from altimeters. This section will incorporate the discussion of three different methods based on data availability. Additionally, it will explain the three approaches derived for these methods: the Bayesian approach when overlap time is present between discharge data and water surface elevation, the quantile approach when it is not and specific approach especially for arctic basins.

The fifth section will describe the procedure to derive river discharge from river width. Using the so-called Non-Parametric Quantile Mapping (NPQM) technique, a data-driven approach that statistically relates the distribution of observed discharge to satellite-based river width measurements, enabling discharge reconstruction even in the absence of simultaneous observations. The NPQM algorithm uses Monte Carlo simulations to generate multiple realizations of discharge and width time series, accounts for measurement uncertainties, and derives a non-parametric mapping function by pairing quantiles of discharge and width without assuming any specific functional form.

The sixth section will describe the procedure to derive river discharge from multispectral images. First, a description on the extraction of reflectance indices is provided along with a multi-mission approach to generate a single time series. Successively, the river discharge estimation is presented based on the similar approaches used for the altimeters (rating curves and quantile approach).

Finally, in section seven, the multi-sensor river discharge approach is presented. Several merging procedures have been considered in previous phase of the project. The selected approach consist of using river discharge at Level-3, which requires the combination of multiple river discharge products independently obtained by the different sensors. The details approach of this product will be provided in the next release of the document (version 2.1).

2 Available ancillary data

An initial analysis of the available data was conducted in WP2 [RD-1] to select stations where the estimation of long-term flow would be particularly valuable and feasible. Since WP2 [RD-1], and specifically during the generation of water height time series using altimetry (WP3.1 [RD-2]), this list of stations has been revised for various reasons, as detailed in the ATBD of WP3.1 [RD-2]. For the remainder of the project, we will investigate a total of 54 stations distributed across 18 different basins (see here: https://climate.esa.int/fr/projects/river-discharge/ and [RD3]). From this updated list, we procured combined time series of water heights dating back to at least 2002, as well as time series from associated missions. In addition to these water height data, observed flow data from various global databases were incorporated:

· **GRDC**: The Global Runoff Data Base (GRDB) maintained by the Global Runoff Data Centre (GRDC) has been the primary dataset used in large-scale hydrological studies, with more than 9000 stations available to the research community (GRDC, 2015). The GRDC is an international archive of data up to 200 years old and fosters multinational and global long-term hydrological studies. Originally established three decades ago, the aim of the GRDC is to help earth scientists analyse global climate trends and assess environmental impacts and risks. https://www.bafg.de/GRDC/

· **AIPo**: The Italian hydrological monitoring network is managed at regional level by different agencies. For the Po basin, the Agenzia Interregionale del Fiume Po (AIPo) is responsible for the coordination of the hydraulic activity, the management and improvement of river navigation infrastructures, environmental and river protection and the coordination of the flood service. For the management of extreme events, AIPo is involved in forecasting and monitoring. Specifically, the website of the agency (https://www.agenziapo.it/content/monitoraggio-idrografico-0) shows real-time and historical measurements that can be freely downloaded by any users.

· **SCHAPI**: In France, in situ gages operated by regional public agencies (i.e. DREALs, Directions Régionales de l'Environnement, de l'Aménagement et du Logement) are collected by the SCHAPI (Service Central d'Hydrométéorologie et d'Appui à la Prévision des Inondations). SCHAPI releases these data publicly via the online "HydroPortail" national database (https://hydro.eaufrance.fr). These public agencies are responsible to observe and forecast floods, and to alert the population in case of dangerous events (https://www.vigicrues.gouv.fr/).

· **SO-HYBAM**: The HYBAM observatory is a unique facility that has been in operation since 2003, with a specialized focus on the monitoring of rivers and water resources in the Amazon region. HYBAM serves as a research support service, conducting extensive and long-term hydrological, sedimentary, and geochemical measurements to gain insights into the origin and evolution of water and transported materials (such as sediments, organic matter, nutrients, etc.) in Amazonian rivers, spanning from the Andes to the Atlantic Ocean. HYBAM collaborates with partners from all countries within the basin and extends its network by including four additional. stations located along rivers that also flow into the tropical Atlantic Ocean: the Orinoco, Congo, Maroni, and Oyapock rivers (https://hybam.obs-mip.fr/fr/donnees/).

· **HYDAT**: Hydrometric data are collected and compiled by Water Survey of Canada's eight regional offices. The information is housed in two centrally managed databases: HYDEX and HYDAT. HYDEX is the relational database that contains inventory information on the various streamflow, water level, and sediment stations (both active and discontinued) in Canada. This database contains information about the stations themselves such as location, equipment, and type(s) of data collected. HYDAT is a relational database that contains the actual computed data for the stations listed in HYDEX. These data include daily and monthly means of flow, water levels and sediment concentrations (for sediment sites). For some sites, peaks and extremes are also recorded. The historical discharge data were extracted from the Environment and Climate Change Canada Historical Hydrometric Data web site https://wateroffice.ec.gc.ca/mainmenu/historical_data_index_e.html

· **ArcitcGRO:** The Arctic Great Rivers Observatory (ArcticGRO) is a collaborative research initiative dedicated to studying and monitoring the hydrology and discharge of some of the largest rivers in the Arctic region. By collecting and analyzing comprehensive data from these rivers, ArcticGRO contributes essential insights into the complex processes and changes occurring in the Arctic's freshwater systems, which are of significant importance in understanding climate change and its effects on the polar environment. The historical discharge data from the ArcticGRO database are available on their official website: https://arcticgreatrivers.org/discharge/.

· **RivDIS:** The Global River Discharge (RivDIS) data set contains monthly discharge measurements for 1018 stations located throughout the world. The period of record varies widely from station to station,

with a mean of 21.5 years. These data were digitized from published UNESCO archives by Charles Vörösmarty, Balaze Fekete, and B.A. Tucker of the Complex Systems Research Center (CSRC) at the University of New Hampshire (Vörösmarty, 1998). River discharge is typically measured using a rating curve that relates local water level height to discharge. This rating curve is used to estimate discharge from the observed water level. The rating curves are periodically rechecked and recalibrated through on-site measurement of discharge and river stage.

· **USGS:** The U.S. Geological Survey's (USGS) supports the acquisition, processing, and long-term storage of water data. Water Data for the Nation serves as the publicly available portal to a geographically seamless set of much of the water data maintained within NWIS. Nationally, USGS surface-water data includes more than 850,000 station years of time-series data that describe stream levels, streamflow (discharge), reservoir and lake levels, surface-water quality, and rainfall. The data are collected by automatic recorders and manual field measurements at installations across the Nation. Data are collected by field personnel or relayed through telephones or satellites to offices where it is stored and processed. The data are processed automatically in near real time, and in many cases, current data are available online within minutes. Streamflow data can be download in the National Water Information System (NWIS) web interface at the following link: http://waterdata.usgs.gov/nwis.

All available data for each station and from all available sources have been merged to constitute observed in-situ discharge (Figure 1).

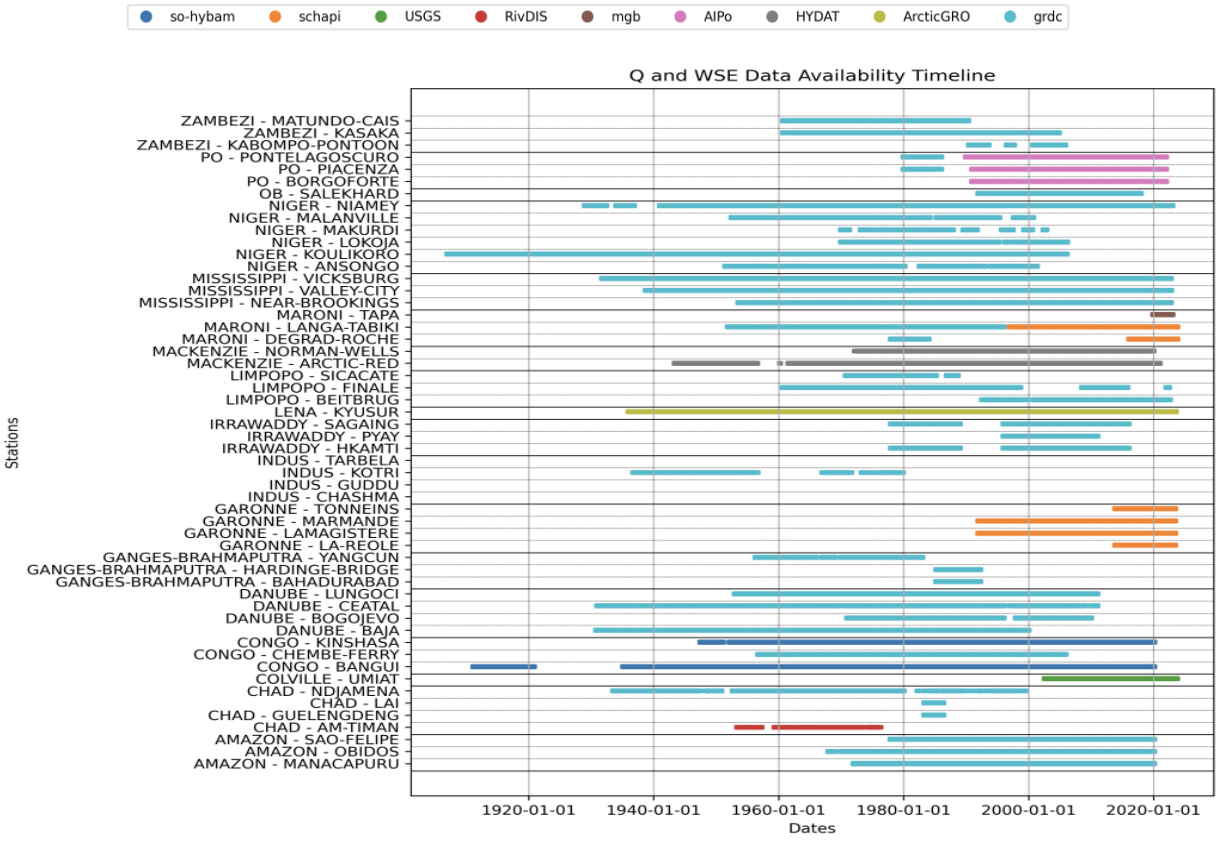

Figure 1: Available discharge data for all stations from different sources

3 Calibration – Validation periods

The methodology used to derive discharge from altimetry WSE will highly depend on ancillary data available and especially discharge time series used for calibration.

The selection of the calibration and validation period for altimeter calibration curves, correlating discharge and water surface elevation, is critically important for result precision. In our approach, we have chosen, in agreement with WP3.1 and WP3.1.2 teams, a method involving the use of the period from the earliest date where simultaneous in situ discharge and merged water surface elevation from the altimeter data (from WP3.1) are available to the latest date when these two data sets overlap (Figure 2). This period is divided into three sections. The first section, in chronological order, is allocated for the validation period, during which altimeter data is compared to reference data to assess model performance. The subsequent two sections are dedicated to the calibration period (Table 1). Using data from these latter two-thirds enables us to take advantage of the most recent satellite constellations and the least biased a priori data, thus ensuring optimal altimeter calibration. This methodological choice is designed to secure the reliability and precision of altimeter measurements across diverse hydrological conditions.

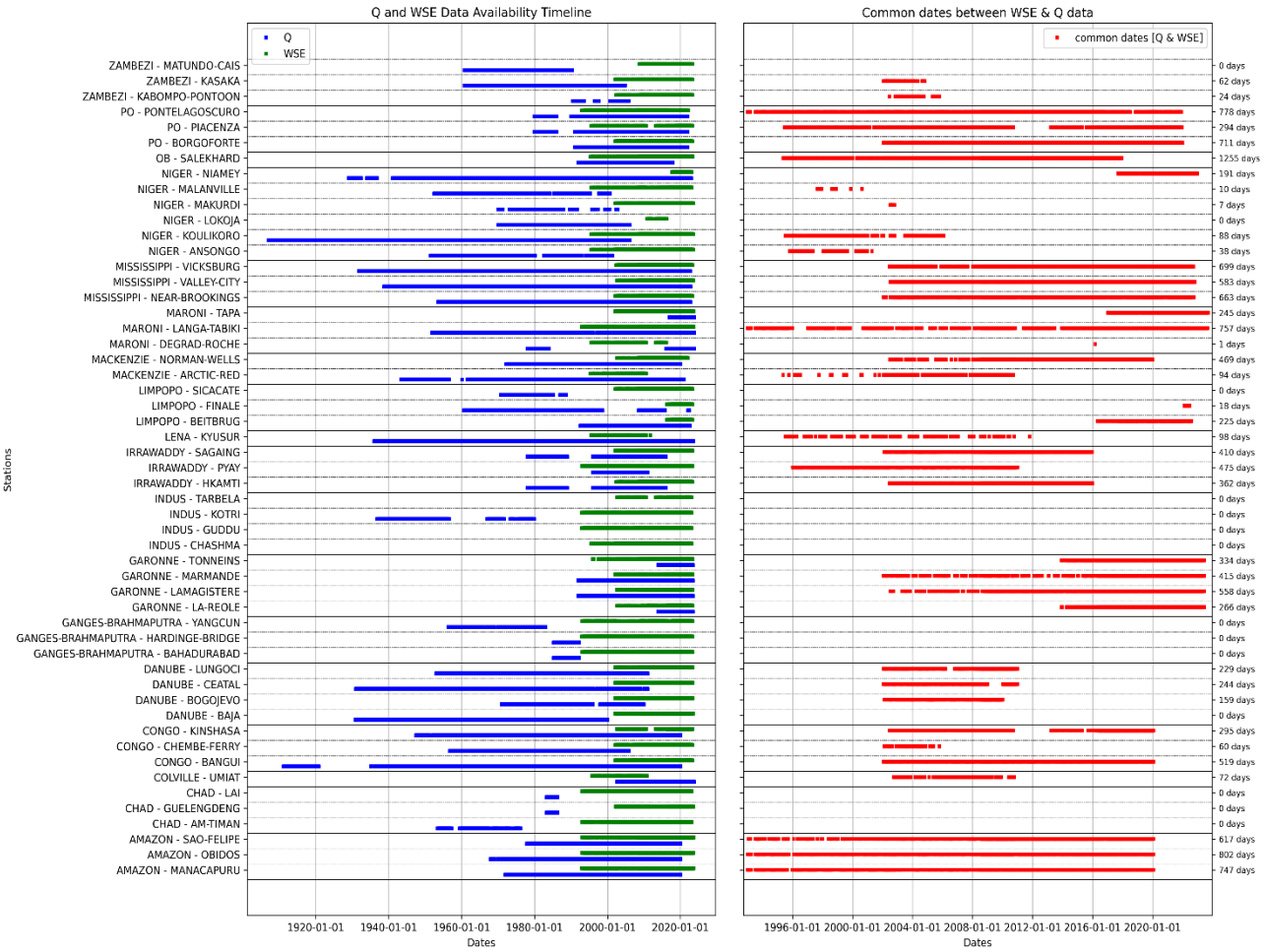

Figure 2: Available data for in situ discharge from various sources (blue) and merged water surface elevation from altimeter (green) from each station. The period where the two data sets overlap is represented in red with the number of overlap's days.

Basins	Stations	Calib sDT	Calib eDT	days	Valid sDT	Valid eDT	days
AMAZON	MANACAPURU	2002-01-05	2020-01-28	548	1992-12-24	2002-01-04	199
AMAZON	OBIDOS	2002-01-08	2020-01-24	599	1992-12-30	2002-01-07	203
AMAZON	SAO-FELIPE	2002-01-19	2020-01-28	529	1993-01-13	2002-01-18	88
CHAD	AM-TIMAN	-	-	-	-	-	-
CHAD	GUELENGDENG	-	-	-	-	-	-
CHAD	LAI	-	-	-	-	-	-
CHAD	NDJAMENA	-	-	-	-	-	-
COLVILLE	UMIAT	2005-05-30	2010-10-10	50	2002-09-22	2005-05-29	22
CONGO	BANGUI	2008-01-29	2020-01-28	377	2002-01-28	2008-01-28	142
CONGO	CHEMBE-FERRY	2003-05-05	2005-10-20	42	2002-02-09	2003-05-04	18
CONGO	KINSHASA	2008-05-05	2020-01-28	235	2002-06-22	2008-05-04	60
DANUBE	BAJA	-	-	-	-	-	-
DANUBE	BOGOJEVO	2004-09-26	2009-12-30	124	2002-02-07	2004-09-25	35
DANUBE	CEATAL	2005-01-08	2010-12-22	161	2002-01-16	2005-01-07	83
DANUBE	LUNGOCI	2005-01-16	2010-12-24	164	2002-01-27	2005-01-15	65
GANGES-BRAHMAPUTRA	BAHADURABAD	-	-	-	-	-	-
GANGES-BRAHMAPUTRA	HARDINGE-BRIDGE	-	-	-	-	-	-
GANGES-BRAHMAPUTRA	YANGCUN	-	-	-	-	-	-
GARONNE	LA-REOLE	2017-02-07	2023-06-09	214	2013-12-07	2017-02-06	52
GARONNE	LAMAGISTERE	2009-06-30	2023-06-10	495	2002-07-10	2009-06-29	63
GARONNE	MARMANDE	2009-03-06	2023-06-10	347	2002-01-17	2009-03-05	68
GARONNE	TONNEINS	2017-02-02	2023-06-10	230	2013-11-29	2017-02-01	104
INDUS	CHASHMA	-	-	-	-	-	-
INDUS	GUDDU	-	-	-	-	-	-
INDUS	KOTRI	-	-	-	-	-	-
INDUS	TARBELA	-	-	-	-	-	-
IRRAWADDY	HKAMTI	2006-12-18	2015-12-24	302	2002-06-14	2006-12-17	60
IRRAWADDY	PYAY	2001-01-02	2010-12-29	320	1996-01-04	2001-01-01	155
IRRAWADDY	SAGAING	2006-09-20	2015-12-19	315	2002-02-03	2006-09-19	95
LENA	KYUSUR	2000-12-11	2011-10-18	63	1995-07-09	2000-12-10	35
LIMPOPO	BEITBRUG	2018-06-04	2022-08-07	175	2016-05-01	2018-06-03	50
LIMPOPO	FINALE	2022-03-25	2022-06-18	11	2022-02-09	2022-03-24	7
LIMPOPO	SICACATE	-	-	-	-	-	-
MACKENZIE	ARCTIC-RED	2000-06-25	2010-09-14	83	1995-05-16	2000-06-24	11
MACKENZIE	NORMAN-WELLS	2008-04-24	2019-12-24	432	2002-06-24	2008-04-23	37
MARONI	DEGRAD-ROCHE *	2016-03-10	2016-03-09	0	2016-03-09	2016-03-09	1
MARONI	LANGA-TABIKI	2003-03-23	2023-09-10	563	1992-12-26	2003-03-22	194
MARONI	TAPA	2021-01-02	2022-12-23	73	2020-01-07	2021-01-01	36
MISSISSIPPI	NEAR-BROOKINGS	2008-12-17	2022-10-02	522	2002-01-24	2008-12-16	141
MISSISSIPPI	VALLEY-CITY	2009-04-12	2022-10-26	492	2002-07-05	2009-04-11	91
MISSISSIPPI	VICKSBURG	2009-03-19	2022-09-20	564	2002-06-17	2009-03-18	135
NIGER	ANSONGO	1997-08-22	2001-04-12	24	1995-10-26	1997-08-21	14
NIGER	KOULIKORO	1999-01-21	2006-01-30	54	1995-07-17	1999-01-20	34
NIGER	LOKOJA	-	-	-	-	-	-
NIGER	MAKURDI *	2002-08-06	2002-10-14	3	2002-07-01	2002-08-05	4
NIGER	MALANVILLE *	1998-08-28	2000-08-20	5	1997-08-31	1998-08-27	5
NIGER	NIAMEY	2019-06-13	2022-12-23	128	2017-09-06	2019-06-12	63
OB	SALEKHARD	2002-11-24	2017-12-10	1194	1995-05-16	2002-11-23	124
PO	BORGOFORTE	2008-09-11	2021-12-23	541	2002-01-19	2008-09-10	170
PO	PIACENZA	2004-04-23	2021-12-19	210	1995-06-24	2004-04-22	84
PO	PONTELAGOSCURO	2002-08-18	2021-12-02	571	1992-12-24	2002-08-17	207
ZAMBEZI	KABOMPO-PONTOON *	2003-07-27	2005-10-20	16	2002-06-13	2003-07-26	8
ZAMBEZI	KASAKA	2002-12-21	2004-10-25	35	2002-01-17	2002-12-20	27
ZAMBEZI	MATUNDO-CAIS	-	-	-	-	-	-

Table 1: Summary of the calibration and validation periods for each station, along with the number of days available for both calibration and validation. Stations marked with an asterisk (*) indicate cases where there is too little overlap between discharge and water surface elevation data to separate into calibration and validation periods. In these instances, all available data will be used for calibration or another method to derive discharge from altimetry will be use.

In instances where there are fewer than 20 common dates between discharge and water surface elevation data, all available data will be utilized for the calibration process, and validation will be conducted by comparing it with alternative data sources, such as in-situ water surface elevation measurements or simulated discharge data generated from modelling.

4 Derive discharge from altimeters (RD-alti)

4.1 Context

Just as in-situ stage measurements can be used to gauge river discharge, altimetry-derived water surface elevation (WSE) can serve as an alternative means of estimating river discharge when discharge time series data is available.

Before selecting the appropriate method, the input WSE data type must be identified:

- WSE-merged (multi-mission altimetry time series): In this case, only the calibration period is retained to compute the rating curve.
- WSE mono-mission (separate altimetry missions): Each mission is processed independently using all available data.

Based on the data sample define by the WSE data type, two main approaches have been used for deriving discharge time series from altimetry observations and supplementary data, depending on the available temporal overlap between discharge and altimetry water surface elevation (WSE) time series.

- **Method 1: Temporal overlap data (preferred approach) -** When sufficient overlapping observations exist, a rating curve is derived by applying the Bayesian method to the paired WSE and discharge data.
- **Method 2: No temporal overlap data (alternative approach) -** When overlap is insufficient or absent, a rating curve is derived by applying the Bayesian method to the quantiles of the full WSE and discharge datasets, assuming stability of the rating curve over time.

To better reflect river-specific conditions and improve the applicability oof rating curves, three main hydrological cases have been distinguished, each associated with adapted versions of these methodologies:

- **Case 1 - General cases**: where we can directly compute the rating curve between the available WSE and Q
- **Case 2 – Rivers with intermittent ice cover:** Filtering ice-affected data points by excluding observations during frozen periods based on temperature thresholds.
- **Case 3 – Arctic rivers**: Arctic and complex hydraulic conditions requiring multiple rating curves for different flow and ice-cover states

4.2 Bayesian-based Rating Curve (RC) estimation

The derivation of rating curves from altimetric water surface elevation (WSE) and in situ or simulated discharge (Q) relies on a Bayesian framework, which allows for robust parameter estimation while accounting for uncertainty (Figure 3).

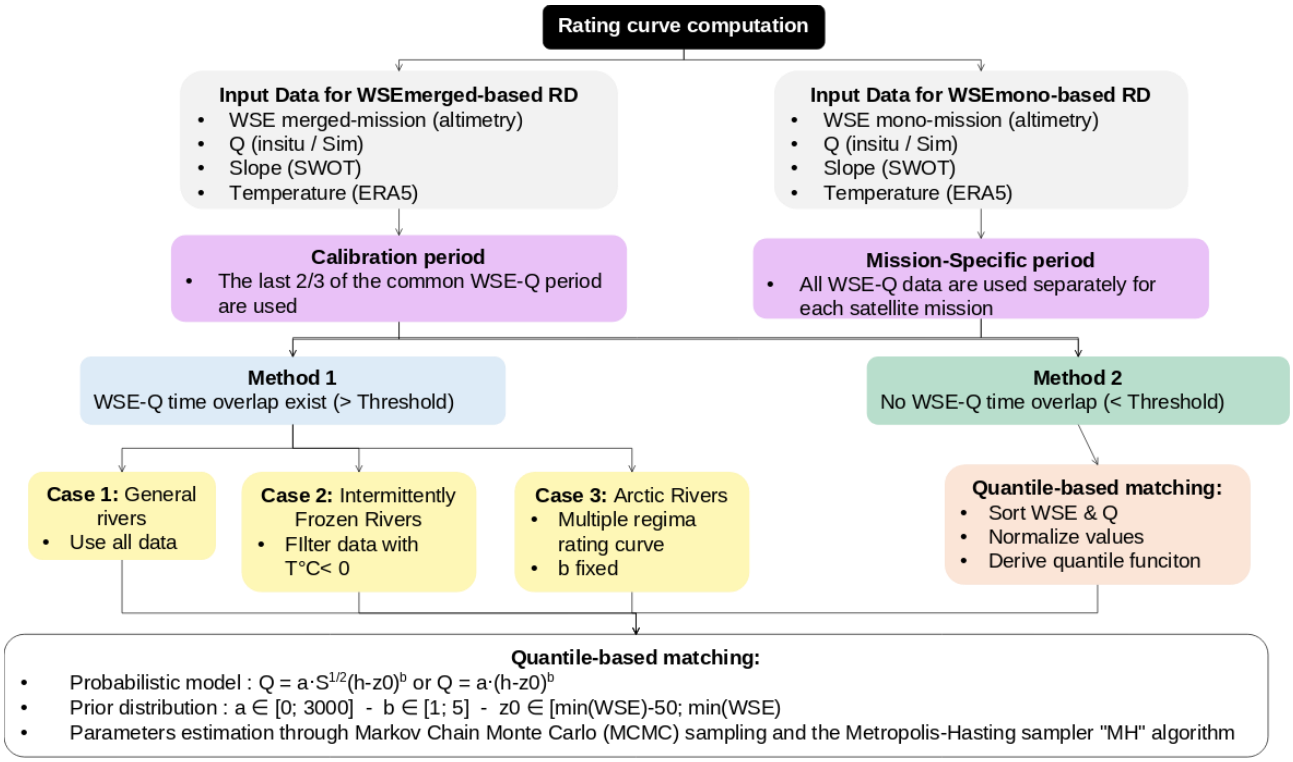

Figure 3: Rating curve computation methodology

4.2.1 Bayesian approach

The Bayesian method is a robust statistical approach used for constructing a rating curve, frequently applied in hydrology when the goal is to estimate unknown parameters from observed data, while considering their associated uncertainty (Gelman et al., 2013). The core of the method relies on Bayes' theorem: (Eq.1):

$$P(\theta/D) = P(D) \cdot P(D/\theta) \cdot P(\theta) \quad \text{Eq.1}$$

Here:

- P(θ|D) is the posterior probability distribution of the model parameters θ, which are the parameters of the rating curve we aim to estimate.
- P(D|θ) is the likelihood of observing the data D, given a specific set of parameters θ, usually based on a probabilistic model.
- P(θ) is the prior probability distribution of the parameters, which incorporates existing knowledge or assumptions.
- P(D) is the marginal likelihood of the data, serving as a normalizing constant to ensure the posterior is a valid probability distribution.

According to this, the estimation of the rating curve using the Bayesian method involves several steps:

4.2.1.1 Rating curve model specification:

The first step consists in defining a probabilistic model that relates observed water surface elevations (WSE) to discharge (Q) through a commonly used power-law relationship:

$$Q = a \cdot (WSE - z0)^b \quad \text{Eq.2}$$

- a is a scaling coefficient controlling the magnitude of the discharge,
- b is an exponent shaping the Q–WSE relationship, reflecting channel geometry and flow regime characteristics (e.g., roughness, cross-section),
- z_0 is the offset or base elevation, generally representing the river bed elevation or the WSE level at which flow begins.

In phase 2 of this study, the rating curve is enhanced by incorporating dynamic water surface slope measurements S, derived from the Surface Water and Ocean Topography (SWOT) mission over few cases as a proof of concept and relevance. The inclusion of slope data is motivated by hydraulic theory, particularly the Manning equation, where discharge depends on both hydraulic radius and slope. The enhanced rating curve equation is formulated as:

$$Q = a \cdot S^{1/2} \cdot (WSE - z0)^b \quad \text{Eq.3}$$

where:

- S is the water surface slope, estimated from SWOT observations, which varies spatially and temporally (trough a climate mean).
- The other parameters retain their physical meaning as before.

This formulation explicitly integrates river slope variability, allowing for a more physically representative and accurate estimation of discharge. It accounts for changes in hydraulic driving forces and improves the adaptability of the rating curve across different river systems and flow regimes.

4.2.1.2 Prior distribution:

The Bayesian framework requires assigning prior probability distributions to each parameter, which can be either informative (based on prior studies or expert knowledge) or uninformative (non-committal). For this study, the following normal prior distributions were adopted, reflecting typical ranges observed in diverse hydrological contexts:

- a (scaling factor):
  - Must be non-negative
  - Typical mean value: 800, standard deviation: 300, resulting in a plausible range: [0 – 1700]
- b (exponent):
  - Must be positive
  - Commonly ranges between 0 and 3 (Chow et al., 1988)
  - Mean: 1.5, standard deviation: 0.5, allowing flexibility for most river geometries and hydraulic conditions
- z_0 (offset or river bed elevation):
  - Estimated as the minimum WSE minus 5 meters (to ensure discharge begins near the riverbed)

- Standard deviation: 5 meters, accommodating variation in channel depth across different rivers (up to ~30 m of flow depth)

- S (slope):
  - Treated as observed input data from SWOT; uncertainties in slope measurements can be incorporated into the likelihood model or modeled as error terms.

These prior distributions are crucial, particularly when dealing with limited or noisy datasets, as they influence the convergence and stability of the estimation process.

4.2.1.3 Posterior estimation and uncertainty quantification:

The final step is the estimation of the posterior distributions of the parameters using Markov Chain Monte Carlo (MCMC) sampling techniques. These distributions provide both point estimates (e.g., posterior means or medians) and credible intervals (e.g., 95% intervals) for each parameter, offering a probabilistic interpretation of the rating curve and its uncertainty.

For this study, the No-U-Turn Sampler (NUTS) algorithm (Hoffman et al., 2014) was selected due to its efficiency in high-dimensional spaces and its adaptive step-size tuning. This advanced variant of the Hamiltonian Monte Carlo (HMC) method ensures faster convergence and better exploration of the parameter space compared to traditional algorithms like Metropolis-Hastings (Robert et al., 2004).

4.2.2 WSE data type

4.2.2.1 WSE merged-mission:

When the water surface elevation (WSE) time series is constructed by merging data from multiple altimetry missions, the rating curve computation is restricted to the calibration period, defined as the last two-thirds parts of the time window where both WSE and discharge data are available (see previous section for details). This period is selected to ensure greater stability in the rating relationship and to avoid early data with potentially lower quality or non-stationary behavior.

If enough paired WSE–Q observations are available within this calibration period, Method 1 (see section 4.2.3) is applied. If not, Method 2 (see section 4.2.4) is used as a fallback.

This approach ensures that the resulting rating curve is based on a coherent, hydraulically consistent subset of the data, improving the reliability of the discharge estimates during the selected period.

4.2.2.2 WSE mono-mission:

In contrast, when WSE data are treated **mission by mission**, as implemented in Phase 2 of the project, all available **common data** between each altimetry mission and the discharge series are used, without restricting to a specific calibration window. This approach acknowledges the sensor-specific nature of each mission and allows for the full exploitation of available paired observations.

For each mission (e.g., Topex/Poseidon, Jason-2, Envisat, Sentinel-3), a separate rating curve is derived. Depending on data availability, either direct pairing (Method 1) or quantile matching (Method 2) is applied individually per mission.

This mission-specific strategy offers several advantages:

- Reduced inter-mission bias, by accounting for the unique characteristics of each sensor;
- Improved temporal resolution, by leveraging the full extent of available WSE–Q pairs for each mission;

- Explicit uncertainty quantification, with posterior distributions computed separately for each mission.

This refined treatment enhances both the accuracy and continuity of discharge estimates across the altimetric record.

4.2.3 Method 1 – Bayesian estimation using overlapping dataset – preferred approach

When a temporal overlap exists between the altimetric water surface elevation (WSE) time series and discharge data (either in situ or simulated), a Bayesian approach can be applied to the paired WSE–Q observations to derive a rating curve. This method is applicable regardless of whether the WSE data comes from a single altimetry mission (WSE mono-mission) or a merged multi-mission time series (WSE-merged), provided that enough synchronous data pairs are available.

To define the sufficient number of synchronous observations needed to compute the rating curve, we base the requirement on the ability to represent seasonal coverage. Specifically, we require data spanning at least 10 distinct months, with each month containing at least 3 points. This criterion ensures that the rating curve is based on a dataset with adequate temporal coverage and density to reliably capture seasonal variability.

The rating curve parameters (commonly denoted as a, b, and $z0$) are estimated using Markov Chain Monte Carlo (MCMC) sampling, allowing the derivation of predictive discharge values along with associated confidence intervals. This approach assumes the WSE measurement location is hydraulically consistent with the discharge reference (e.g., colocated or in a reach with stable morphology), and that river conditions remain relatively stationary during the calibration period.

This method has been widely adopted in recent literature (e.g., Garambois et al., 2017; Domeneghetti et al., 2014; Paris et al., 2022) and is well suited to rivers without major non-stationarities such as ice cover or abrupt morphological changes.

However, in real-world applications, river dynamics may not always support the direct application of this method due to seasonal ice effects or non-uniform flow behaviors. To address these situations, we define three specific cases for the construction of the rating curve:

4.2.3.1 Case 1 – General rivers

In this case, a standard Bayesian rating curve is computed directly from all available overlapping WSE–Q pairs. No filtering of the time series is needed, and the full dataset is assumed representative of the hydraulic behavior. This case applies to rivers without significant freeze/thaw effects or strong interannual variability in seasonal patterns.

4.2.3.2 Case 2 – Partial ice cover rivers

In some river systems, particularly in temperate cold climates, ice cover appears only intermittently, typically during winter months (e.g., December to March), and varies from year to year. This irregular freezing can create outliers or distortions in the WSE–Q relationship during those periods.

To mitigate this, the overlapping dataset is filtered using a temperature threshold: WSE–Q pairs associated with monthly mean air temperatures below 0°C are excluded. For instance, at the Near-Brookings station, the river was frozen in some winters, producing anomalies in the WSE–Q scatter plot.

By applying ERA5 monthly temperature data, periods of likely ice presence were identified and removed, resulting in a more consistent rating curve.

This filtering allows the construction of a more representative and robust rating curve, avoiding the influence of anomalous hydraulic states induced by ice, while maintaining a unified Bayesian framework.

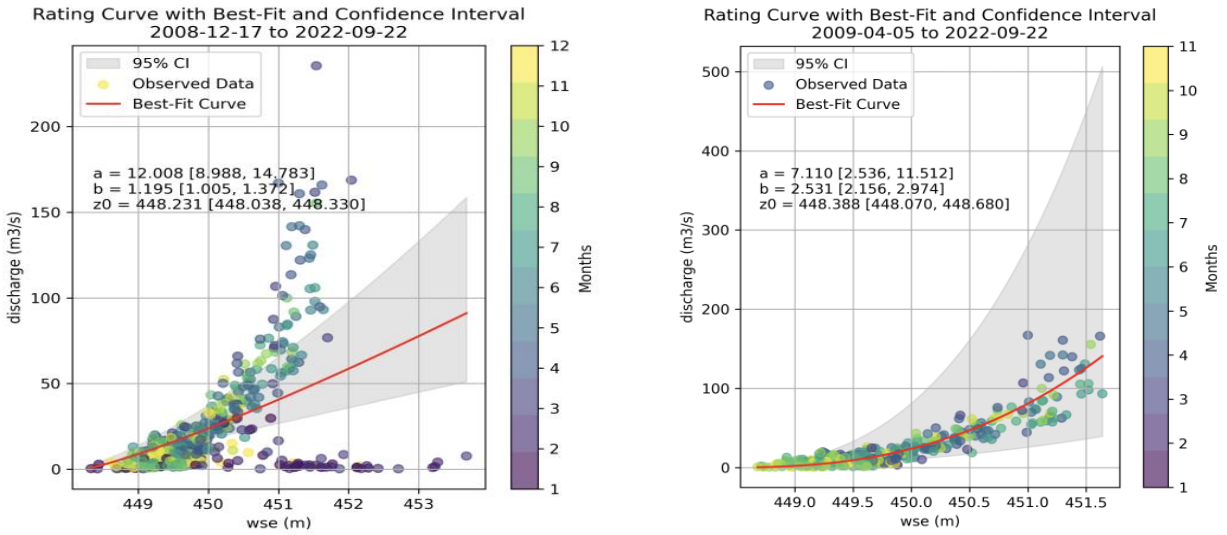

Figure 4: Rating curve for the Near-Brookings station (Mississippi basin) before (left) and after (right) excluding data points associated with temperature variations (below 0°C).

4.2.3.3 Case 3 – Artic rivers

In Arctic regions, the relationship between water surface elevation (WSE) and discharge is often non-uniform due to seasonal ice cover, ice breakup, and complex flow dynamics near river confluences. In such contexts, a single rating curve may be inadequate. Instead, a set of rating curves, each tailored to a specific hydrological regime—such as flood rise, recession, or ice-covered periods—is employed. This approach requires prior knowledge of the river's seasonal behavior and the applicability range of each curve.

The impact of river ice on flow hydraulics can be detected using remote sensing and altimetry observations acquired simultaneously with WSE retrievals (Zakharova et al., 2021). Previous studies have demonstrated that using distinct rating curves for different flow conditions improves discharge estimation accuracy (Zakharova et al., 2020). Classical power-law equations are used for flood rise and recession periods, while low-degree polynomials may better capture the hydraulic behavior during the ice-covered period.

For example, on the Ob River, an automated method based on altimetry was tested to detect ice-on and ice-off periods from 2008 to 2019, which enabled the calibration and validation of a winter-specific rating curve. For years not covered by this product, optical imagery from Landsat and MODIS was used. The spring flood rise subset was extracted directly from the WSE time series. On four Arctic test sites—located on the Colville, Mackenzie, and Lena rivers—two rating curves were built using a modified Bayesian method: one for flood recession, and another combining winter and flood rise periods. In this modified method, only the parameters "a" and "z_0" were estimated probabilistically, while the exponent "b" was fixed to allow expert adjustment of the curve shape for each hydrological regime.

This regime-based approach enhances discharge estimation in Arctic environments by accounting for seasonal variability in flow hydraulics and by leveraging multi-source satellite data.

4.2.4 Method 2 – Bayesian estimation using quantile-based matching – alternative approach

The quantile-based approach is a statistical modelling technique used to derive a rating curve by matching quantile functions of water surface elevation (WSE) and discharge time series. Unlike the Bayesian approach, it does not require a temporal overlap between altimetry observations and in situ discharge measurements. This makes it especially valuable when satellite data and discharge records originate from distinct periods. The method has been successfully applied across a range of river basins in various climatic zones—including the Amazon, Brahmaputra, Danube, Niger, and Ob rivers (Tourian et al., 2013).

4.2.4.1 Theoretical Framework

This method assumes that river flow behavior is stationary over time and that the bathymetry remains stable both at the virtual altimetry station and the in-situ gauging station. Under these conditions, historical in situ discharge data can be validly used to estimate present-day discharges derived from satellite altimetry.

The foundation of the approach lies in the construction of quantile functions:

$$Q_{\mathrm{R}}(p) = \inf\{X_{\mathrm{R}} \in R : p \leq F(X_{\mathrm{R}})\} \quad \text{Eq.4a}$$

$$Q_{\mathrm{W}}(p) = \inf\{X_{\mathrm{W}} \in R : p \leq F(X_{\mathrm{W}})\} \quad \text{Eq.4b}$$

where:

- $Q_R(p)$, is the quantile function of in situ discharge values X_R
- $Q_W(p)$, is the quantile function of altimetric WSE values X_W
- $F(\cdot)$ denotes the cumulative distribution function (CDF),
- and $p \in (0,1)$ is the exceedance probability.

The quantile function $Q(p)$ returns the maximum value of the variable that is not exceeded with probability p. It provides a distribution-free description of the data, enabling the definition of a functional transformation $T(\cdot)$ between the two datasets:

$$Q_{\mathrm{R}} = T(Q_{\mathrm{W}}) \quad \text{Eq.5}$$

This transformation is assumed to be **monotonic and non-decreasing** (Gilchrist, 2000), a key requirement that allows for a meaningful functional relationship between WSE and discharge. Since this formulation does not rely on time-matching between datasets, it is ideal for scenarios without temporal overlap.

4.2.4.2 Practical Implementation

To empirically estimate the quantile functions, each dataset (WSE and Q) is sorted in ascending order. The rank k_i of each value is normalized as:

$$p_i = \frac{k_i}{N+1} \quad \text{Eq.6}$$

N is the number of measurements, and p_i is the empirical probability associated with each sorted value. This produces two ordered series of quantiles (WSE and Q), which are then paired to create a scatter plot of discharge quantiles versus WSE quantiles.

The quantile functions can be constructed:

- using mean monthly discharge and WSE (based on historical daily discharge and satellite observations at altimeter passes), as in Tourian et al. (2013),
- or by matching altimetric WSE values at satellite overpasses with daily discharge values in the historical dataset, to better reflect short-term flow variability, including extreme events.

This second variant has been explored in this study to overcome the limitations of monthly mean values, which may obscure significant hydrological fluctuations. By doing so, the derived rating curve incorporates more of the inherent non-stationarity of river flow, offering a better match between satellite-derived WSE and hydrological dynamics.

4.2.4.3 Application and Comparison

Both the monthly-based and daily-based quantile pairing approaches are tested in this work to build rating curves during periods without temporal overlap between WSE and Q datasets. These curves are evaluated in Work Package 4.2.

In both cases, the quantile space is discretized using an equidistant step of 5%. The resulting quantile–quantile scatter plots are used as input for a Bayesian inversion, following the same procedure described in Section 4.2.1, to derive the final rating curve parameters.

This method is applied both to merged multi-mission altimetry WSE time series and to each individual altimetry mission, to evaluate the contribution and uncertainty associated with each data source. The mission-specific analysis may enhance discharge estimation accuracy for missions with better precision or denser temporal coverage.

4.3 Uncertainties

Uncertainty propagation through mathematical models plays a crucial role in estimating the reliability of derived results in various scientific fields. In the context of hydrology and discharge estimations, the propagation of uncertainties in parameter estimation, such as those in the parameters of the discharge equation, becomes essential for assessing the reliability of the calculated discharge values. Utilizing a Gaussian error propagation method provides a systematic approach to quantify the uncertainties associated with parameters a, WSE, b, and z0 (and s if available) from the power law function defined in section 4.2.1 to express the relation between Q and WSE.

This method involves employing statistical principles to propagate uncertainties through the mathematical relationships between the parameters and the discharge equation. By considering the Gaussian distribution of errors in these parameters, this approach enables a more comprehensive evaluation of the overall uncertainty in discharge estimations (e.g., McMahon and Peel, 2019, Tourian et al., 2017).

Given the mean values and standard deviations (σ) for each parameter, the uncertainty in discharge (δQ) due to uncertainties in these parameters can be computed as Eq.7 if the slope value is unknow otherwise as Eq.8:

$$\partial Q = \sqrt{\left(a\cdot(WSE-z0)^{b}\cdot\sigma a\right)^{2}+\left(a\cdot b\cdot(WSE-z0)^{b-1}\cdot\sigma WSE\right)^{2}+\left(a\cdot(WSE-z0)^{b}\cdot\ln(WSE-z0)\cdot\sigma b\right)^{2}+\left(-a\cdot b\cdot(WSE-z0)^{b-1}\cdot\sigma z0\right)^{2}} \quad \text{Eq.7}$$

$$\partial Q = \sqrt{\left(a\cdot\sqrt{S}\cdot(WSE-z0)^{b}\cdot\sigma a\right)^{2}+\left(a\cdot\frac{1}{2\sqrt{S}}\cdot(WSE-z0)^{b}\cdot\sigma s\right)^{2}+\left(a\cdot\sqrt{S}\cdot b\cdot(WSE-z0)^{b-1}\cdot\sigma WSE\right)^{2}+\left(a\cdot\sqrt{S}\cdot(WSE-z0)^{b}\cdot ln(WSE-z0)\cdot\sigma b\right)^{2}+\left(-a\cdot\sqrt{S}\cdot b\cdot(WSE-z0)^{b-1}\cdot\sigma z0\right)^{2}} \quad \text{Eq.8}$$

Where, σa, σb, σz0, σs and σWSE correspond to the standard deviations of parameters a, b, z0, S and WSE respectively. The standard deviations for a, b, and z0 will be determined using the Bayesian approach through the MCMC algorithms (see section 4.2.1). The standard deviation for the WSE will be, initially, consistent across all stations and for each mission. This value will later be adjusted through updates during the validation process. The standard deviation for the slope will be define as the standard deviation per month over the 2 years of available data.

This formula uses the standard deviations as measures of uncertainty in each parameter and calculates the overall uncertainty in discharge considering the propagation of these uncertainties through the power law equation relating discharge and the parameters *a, b, z0, S and WSE*.

It is important to notice in one hand, that this equation assume that the uncertainties in the parameters (a, b, z0) and WSE are independent, and in another hand, that the propagation of uncertainties provides an estimate based on the assumption of linearization around the mean values of the parameters.

5 Derive discharge from river-width (RD-width)

5.1 River width estimation using optical satellite imagery

Following the methodology introduced by Elmi and Tourian (2023), this algorithm estimates river width from time-series satellite imagery (Landsat 8/9 and Sentinel-2) using water indices, topographic constraints, and a graph-based image segmentation framework that incorporates spatial smoothness and temporal dependency. A river reach is first selected from the SWOT River Database (SWORD) and buffered based on its mean width and standard deviation to define an analysis zone. Only pixels satisfying slope, elevation, and water occurrence thresholds (from FABDEM (Forest And Buildings removed Copernicus DEM) and Global Surface Water Explorer (GSW) (Pekel et al. 2017)) datasets) are retained for analysis. After applying rigorous cloud masking and computing water indices such as Normalized Difference Water Index (NDWI), the image time series is smoothed and normalized within each step. As in Elmi and Tourian (2023), the water index is combined with a long-term water occurrence map via a sigmoid function to enhance temporal consistency. The result is a probability map representing the likelihood of water presence at each pixel and time step.

Segmentation is then performed using a maximum-flow/minimum-cut algorithm that operates on a graph constructed over each probability map. Each pixel is treated as a node connected to source and sink terminals (representing water and non-water classes), with edge capacities determined by the pixel-wise water probability.

Let $\mathcal{L}$ denote the set of pixels in the buffered river region and assign a binary label $f_p \in \{0,1\}$ to each pixel $p \in \mathcal{L}$, where $f_p = 1$ represents water and $f_p = 0$ represents non-water. The goal is to find a labeling that minimizes the energy:

$$E(f) = \sum_{p \in \mathcal{L}} D_p(f_p) + \lambda \sum_{(p,q) \in \mathcal{N}} V_{p,q}(f_p, f_q) \quad \text{Eq.9}$$

where:

-$D_p(f_p)$is the data term (unry potential), encoding the likelihood that pixel p belongs to class f_p.

- $V_{\{p,q\}}(f_p, f_q)$ is the smoothness term (pairwise potential), enforcing spatial coherence.

- λ > 0 is the regularization term.

- $\mathbb{N}$ is the number of 4-connected pixel neighbors around the border

The term $D_p(f_p)$is the cost function defined in the temporal domain, which can be obtained from the monthly or long-term water occurrence map from GSW that delivers the probability of water in a certain pixel P_p. So:

$$D_p(f_p) = \begin{cases} P_p & \text{if } f_p = 1 \quad \text{(label: water)} \\ 1 - P_p & \text{if } f_p = 0 \quad \text{(label: non-water)} \end{cases} \quad \text{Eq. 10}$$

On the other hand, the smoothness term $V_{p,q}(f_p, f_q)$ penalizes discontinuities between neighboring pixels based on water index similarity:

$$V_{p,q}(f_p, f_q) = 0 if f_p = f_q, \exp(-|I_p - I_q|/\sigma) if f_p \neq f_q \quad \text{Eq. 11}$$

To solve the energy minimization problem defined by the binary labeling function f_p, we employ the Max-Flow/Min-Cut algorithm. The formulation is cast as a graph cut problem, where each pixel corresponds to a node in a directed graph, and two additional nodes represent the source (water) and sink (non-water). The edge weights are derived from the data and smoothness terms: terminal links (T-links) encode the data cost $D_p(f_p)$, while neighborhood links (N-links) encode the pairwise smoothness cost $V_{p,q}(f_p, f_q)$. The Max-Flow algorithm (implemented using the PyMaxflow library) computes the minimum s–t cut that separates the graph into water and non-water regions, yielding the optimal binary segmentation f* that minimizes the total energy. This approach guarantees a globally optimal solution for binary segmentation under submodular energy terms.

5.2 River discharge estimation using river width

A complementary approach to traditional discharge estimation using hydraulic or hydrological models is the use of satellite-derived river width time series as a proxy for in-situ discharge observations. We apply a non-parametric, data-driven technique called Non-Parametric Quantile Mapping (NPQM) (Elmi et al. 2021) to estimate river discharge from width time series extracted from optical satellite imagery (section 5.1). The approach allows for discharge estimation at river reaches near selected gauges, even in the absence of simultaneous observations. By building a statistical relationship between the distribution of

observed river discharge and EO-based river width, this method can reconstruct discharge time series that are consistent with long-term flow characteristics.

The flowchart below outlines the core steps of the NPQM algorithm for estimating discharge from river width:

- First, the algorithm generates multiple realizations (simulations) of both the in-situ discharge and satellite-derived river width time series using Monte Carlo simulation. These simulations account for the uncertainties in the original measurements.
- Then, for each realization, it builds a set of mapping functions by pairing all possible combinations of discharge and width quantile values (see Eq.4a, Eq.4b, and Eq.5, note that in Eq.4b instead of wse, we use river width).
- Once the mapping functions are created, the algorithm calculates the mean river width- discharge mapping function for each percentile, as well as the associated uncertainty. The non-parametric mapping function is obtained without assuming a specific functional form.
- To assess the accuracy of the mapping, the model compares the estimated discharge values with observed discharge values. A "3-sigma test" is used, which checks whether the differences between estimated and observed discharges fall within three standard deviations—capturing about 99.7% of the values in a normally distributed dataset. If simultaneous discharge and width data are available, they are used directly; otherwise, the comparison is made using data that fall within the same quantile range.
- Based on the outcome of the 3-sigma test, the algorithm adjusts the uncertainty of the measurements to maintain consistency in an iterative process.
- The algorithm then checks whether the Root Mean Squared Error (RMSE) has changed significantly compared to the previous iteration. If not, the model stops. If it has, the process adjusts the uncertainty and repeats from the first step.

At the beginning of the process, a default uncertainty of 10% of the signal is assumed for both discharge and width time series, due to the limited availability of formal uncertainty estimates. As the iterations proceed, this uncertainty is refined based on the model's performance. Once the model has converged, it can be used to estimate discharge values—with associated uncertainties—based solely on the input river width time series. Further information on the uncertainty treatment and validation of the NPQM method is available in Elmi et al. (2021, 2024), where the algorithm is applied and analysed in depth using both water level and width datasets.

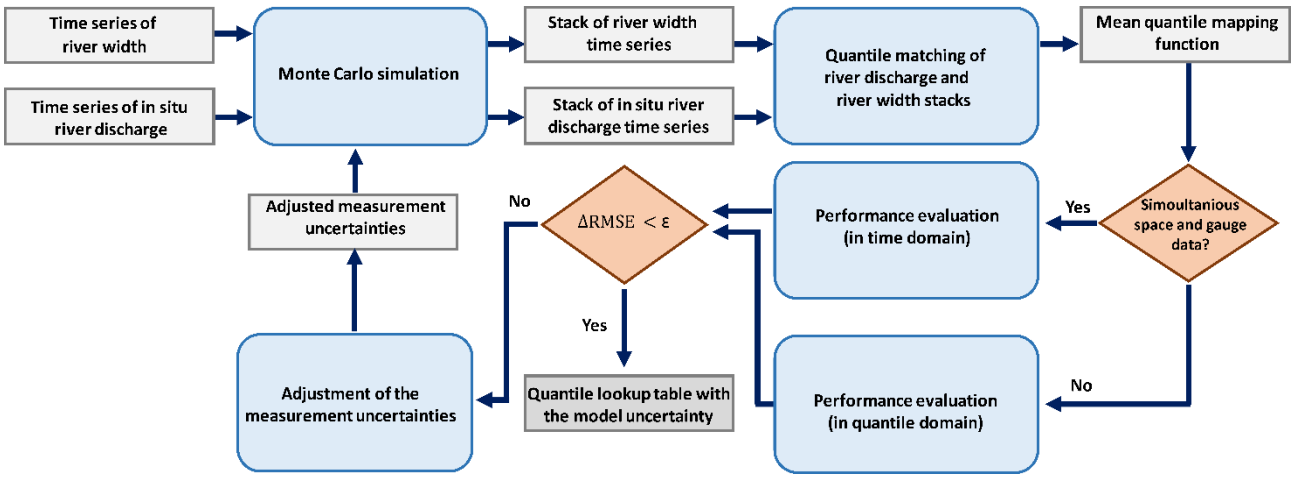

Figure 5: Flowchart of the stochastic quantile mapping function algorithm (adapted from Elmi et at., 2021, and Saemian et al., 2024)

6 Derive discharge from multispectral images (RD-multispec)

6.1 Context

The method for estimating river discharge from multispectral images is based on the studies of Tarpanelli et al. (2013), Filippucci et al. (2022) and Filippucci et al. (2025), in which the differences between the passive response of the reflectance signal from the soil and that from the water are used to identify a change in the land area near the river channel that is shown to be strongly correlated with river discharge. An increase in river discharge produces an increase in wetted area, and the area near the river changes its reflectance response, which decreases. For an area near the river that is not affected by water, reflectance remains almost constant (except for changes in vegetation cover). Its relationship with the reflectance of the wetted area is used to more accurately determine the estimate of changes in hydrologic forcing, compared to the wetted area alone. Consequently, in the case of flooding, the reflectance ratio between the dry pixel (called the calibration pixel, C) and the wet pixel (called the measurement pixel, M) is sensitive to the increase of water in the wet pixel and, therefore, is directly related to the increase of river discharge. With respect to the first study by Tarpanelli et al. (2013) where the reflectance ratio C/M has been extracted from a temporal series of seven years of almost daily images of MODIS over four stations along the Po River, the analysis by Filippucci et al. (2022) demonstrated that the role of sediments and vegetation in the formulation was important to correct the reflectance ratio C/M during flood events. This was possible with the use of finer resolution images from Sentinel-2 and the new approach was tested over two Italian rivers, Po and Tiber. In Filippucci et al. (2025), the selection of reflectance indices based on local hydrological conditions is carried out evaluating the best procedure to obtain river discharge proxies according to the specific flow regimes and climatic conditions across 54 sites worldwide.

6.2 Reflectance indices definition

In the project, we tested several algorithms for the estimation of the reflectance index. Such algorithms come from the combination of pixels: C for calibration, W for the sediments, V for the vegetation, M for measurements of the variation. The main steps for the application of the procedure are listed below:

- The study area is predetermined as a square of fixed side (e.g. 0.04 degree for Sentinel-2 data, 0.06 degree for Landsat data and 0.15 degree for MODIS data) around the selected station.
- The collection of the desired data in the chosen area is then obtained for the available period.
- Cloud products are considered to mask the cloud presence in the single images. After this masking, the total number of valid pixels in each image is computed. If the fraction of valid pixel was less than 0.2, the full image was discarded. Similarly, the fraction of valid reflectance value was calculated for each pixel during the study period: if this value was below 5%, the pixel was deemed invalid and removed by the analysis, to avoid its selection in the mask calculation.
- Snow or ice presence is masked through other products available in the collection of data. The fraction of snow pixels is calculated for each available image and the resulting time series is averaged for each day of the year, to obtain a standard year probability of snow presence. A windowed moving average filter of 14 days was then applied to reduce the noises.
- Water area pixels are obtained using JRC Global Surface Water Mapping Layers for coarse resolution sensors (MODIS and Sentinel-3) and the application of a threshold to the 5th percentile of NDVI timeseries for the remnant products. For each image, if the fraction of valid pixels in the water area was less than 0.2, the full image was discarded.
- The different categories of pixels (vegetation, bare soil and field) are classified through masks derived by NDVI index, coefficient of variation (NIR standard deviation divided by NIR average), mean and standard deviation.

- The final step consists in the selection of the periodically wet area. When observed data concurrent to satellite overpass are available, four algorithms of the reflectance indices are calculated to be compared with the in situ river discharge: the pixels with highest Spearman's correlation are selected as M. When observations are not available, two uncalibrated procedures are adopted, one based on the correlation between the pixels within the water area and the different categories, and one based on the JRC Global Surface Water Mapping "Occurrence" information.

Different formulations of the proxy are adopted according to the characteristics of each river reach (e.g. application of vegetation and sediment correction; use of multiple water mask selection algorithms) and satellite pixels may be aggregated for stations where the river width is considerably larger than the satellite spatial resolution (especially when we use Landsat and Sentinel-2).

Moreover, because the analysis involved long temporal period, we need to consider the natural evolution of the river morphology. This means that in some areas a static temporal analysis that considers the same pixels for the entire period is not sufficient to describe the dynamic of the river. In such cases it is necessary to perform the analysis for brief periods. Therefore, the procedure was applied two years in two years, maintaining one year in common between a period and the following one, in order to avoid big changes in the transition period. The pixel categories masks were obtained combining the ones of the single periods. The procedure, called "multi-year", is used along with the "full period" for evaluating the benefit to separate the period with respect to the static investigation.

Based on what we describe above, the total number of algorithms to be considered in the analysis is 24 to be applied to the 11 satellite products.

6.3 Multi-mission reflectance time series

A total of 24 calibrated reflectance indices were obtained for each station considering all formulations (CM, CMW1, CMW2), aggregation kernels (one small and one large), vegetation correction and calibration type (full or multiyear). A first analysis is then necessary to identify the best algorithm for the definition of river discharge. This discrimination is carried out based on a stepwise maximization of the Spearman correlation coefficient, to consider the non-linearity between the reflectance index and the river discharge. Because the procedure includes several combinations, we proceed to distinguish for each satellite products the following sub-cycles:

1- the best temporal method between full period and multi-year;
2- the best spatial resampling of the images with the aggregation;
3- the best formulation between the simple C/M or the ingestion of the sediments with CMW;
4- the best formulation with the inclusion of the vegetation

This stepwise procedure allowed to obtain two results: first, the best calibrated procedure was obtained for each station, second, the analysis of the results combined with the stations characteristics allowed to obtain a heuristic procedure to obtain a valid algorithm for each station in the uncalibrated procedure.

The application of the above methodology to the 10 datasets investigated in this project allows to obtain 10 different timeseries related to river discharge in 54 and 26 stations using the uncalibrated and calibrated procedure, respectively. The indexes were then merged together to obtain a single consistent signal from multispectral sensors (one for the calibrated and one for the uncalibrated methodology). This procedure is complicated by the fact that most of the sensors have different spatial resolution, coverage period and revisit time. A summary of the different dataset characteristics is shown below.

Platform	Product	Reflectance	Platform	Start year	End year	Spatial resolution	Revisit time
Landsat 5	L2, C2, T1	TOA	GEE	1984	2013	30 m	16 d
Landsat 7	L2, C2, T1	TOA	GEE	1999	2022	30 m	16 d
Landsat 8	L2, C2, T1	TOA	GEE	2013	-	30 m	16 d
Landsat 9	L2, C2, T1	TOA	GEE	2021	-	30 m	16 d
MODIS TERRA	MOD09GQ	TOA	GEE	1999	-	230 m	1 d
MODIS AQUA	MYD09GQ	TOA	GEE	2002	-	230 m	1 d
Sentinel 2	S2-L1C	TOA	GEE	2015	-	10 m	5 d (10)
Sentinel 2	S2-L1C	TOA	SH	2015	-	10 m	5 d (10)
Sentinel 2 + Landsat 8-9	-	TOA	SH	2015	-	30 m	3-4 d
Sentinel 3 OLCI	S3-L1B	TOA	SH	2016	-	300 m	~1 d
MERIS	-	-	EC	2002	2012	300 m	1 d

Table 2: Description of the datasets for multispectral images. It includes selected product, reflectance type, platform used to analyze the data (GEE is Google Earth Engine, SH is Sentinel-HUB, EC is Earth Console), period of data availability, spatial resolution and revisit time.

Some datasets share data from one or more sensors (e.g. S Sentinel- 2 in Google Earth Engine (GEE) and Sentinel-2 in Sentinel Hub (SH)). To avoid using more than one time the same data, three different combinations were considered for the merging:

Landsat 5-7-8-9; Sentinel 2 (GEE) – 3; MODIS TERRA and AQUA; MERIS

Landsat 5-7-8-9; Sentinel 2 (SH) – 3; MODIS TERRA and AQUA; MERIS

Landsat 5-7-8-9; Sentinel 2 (GEE) – 3; MODIS TERRA and AQUA; MERIS

It should be also noticed that some sensors may be not able to obtain reliable river discharge information over specific rivers due to insufficient spatial resolution (when river width << sensor's spatial resolution), fail of the uncalibrated procedure (impossibility to obtain C or W due to sensor's spatial resolution or specific characteristic of the river) or other reasons. Therefore, it is important to exclude bad performing data from the merging to avoid worsening the performance. For the calibrated stations, all the datasets with Spearman correlation with observations < 0.4 will be therefore excluded by the merging. For the uncalibrated procedure, where also stations with non-concurrent data were considered, this strategy is not applicable. Therefore, first the CM index will be averaged to obtain a monthly timeseries, then the CM of each single month (January, February…) will be averaged together to obtain a monthly standard-year CM index. The Spearman correlation between this index and the corresponding monthly standard-year observed data (considering also non-concurrent periods) will be calculated and considered as a good estimator of the actual Spearman correlation of the calibrated timeseries (). A categorical score analysis was then carried out to obtain the best monthly Spearman correlation threshold () able to reproduce the condition in which the calibrated Spearman correlation in less than 0.4: for each potential threshold it was calculated the Probability of Detection (POD), False Alarm Ratio (FAR) and Threat Score (TS), considering:

$$POD = \frac{A}{A + C}$$ Eq.12a

$$FAR = \frac{B}{A + B}$$ Eq.12b

$$TS = \frac{A}{A + B + C}$$ Eq.12c

With:

	$S_c < 0.4$	$S_c > 0.4$
$S_m < S_t$	A	B
$S_m > S_t$	C	D

The results of this analysis will be exploited to obtain the correct S_t to be applied in the uncalibrated procedure, also ensuring the selection of at least one daily timeseries (MODIS AQUA, TERRA or S3) or 3 different products. If this condition is not obtained, all the products of the selected combination will be selected for the merging.

Once the products to be merged have been selected, the first operation to be done is rescale all the satellite data to a reference scale. The product with the highest amount of available data is chosen as reference. All the products are hence scaled to this one. First the number of overlapping data is calculated. If this is greater than 5, the minimum and 75th percentile of the selected product and the reference one is calculated, and the product is rescaled according to (Eq.9):

$$P_i^s = \frac{P_i - m}{p75 - m} \cdot (p75^r - m^r) + m^r$$ Eq.13

Where P_i is the i-th element of the selected product, P^s_i is the same element scaled to the reference, p75 and m are the minimum and the 75th percentile of the selected product, respectively, calculated during the overlapping days, and $p75^r$ and m^r are the same for the reference product. In case less than 5 overlapping days between the reference and the selected datasets are available, the minimum and 75th percentile are calculated for the whole period for both the selected and reference products. It is worth underlining that it was decided to use the 75th percentile instead of the more common maximum value to avoid selecting potential outlier due to errors in the cloud masking or presence of cloud shadow. Potential outliers are then eliminated by removing all the data index greater than 10 or less than 0. The merging procedure is finally carried out: all the data is interpolated at daily steps. A weight is assigned to each daily data, proportional to the distance from the sensing date: the weights are assigned according to the gaussian distribution, fixing w=1 in the sensing date, w=0.5 at three days from the sensing date (figure 6). All the interpolated data at more than 6 days from the sensing date are fixed to NaN. Then, the potential presence of contradictory information from the different sensor is accounted for by calculating the difference between the maximum and minimum value of the index for each day of the analysis (considering all the products). The distribution of this variability is assumed as gaussian (excluding data in which only one sensor is available, and the max-min difference is equal to 0): the average and the standard deviation of the max-min difference is calculated and all the dates outside the 3 times standard deviation range are excluded from the analysis. Finally, the weighted sum is performed by maintaining only the dates in which one or more products has w=1 (at least one product is obtained in that date). An exponential filter with T=6 is then applied to remove possible noises.

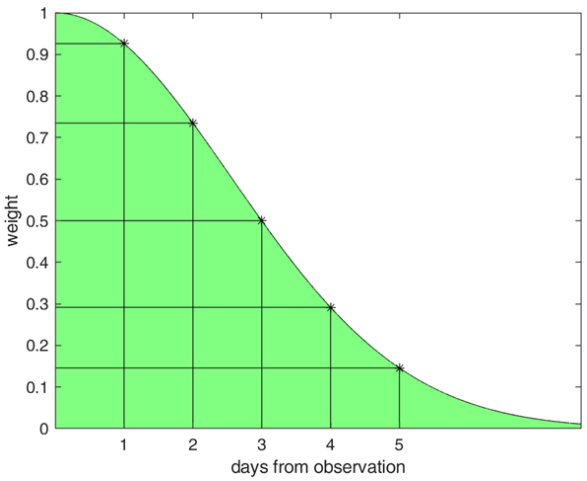

Figure 6: Weights of the daily data of each sensor according to the temporal distance by the nearest sensing day. The weights are distributed with a gaussian function River.

6.4 River discharge estimation from reflectance indices

The estimation of river discharge from reflectance indices is very similar to the rating curve approach applied for the water levels by altimetry. Indeed, here the relationship is based on the evaluation of a non-linear regression relationship between the multi-mission time series and the observed river discharge values. After processing the multispectral images from the multi-mission satellites following the methodology explained in Section 5.3, the retrieved signals (hereafter denoted as CM signals) are further utilized to derive river discharge time series along the selected river reaches. To formulate the river discharge algorithm, we need to calibrate the CM signals against the contemporary in situ river discharge for any typical river sites. However, along the selected river sites, the in situ observations are often unavailable during the period in which satellite data are available (2006-2005 for Landsat 5, 2021-2022 for Landsat-9, 2016-2022 for the remnants). Therefore, two different analyses are carried out depending on the availability of the in situ data: i) calibrated approach (when coincident observation of in situ Q and CM signals are available) and ii) uncalibrated approach (when only in situ observation non-contemporary to satellite data are available).

6.4.1 Calibrated Approach

With the coincident data availability of CM and Q, River discharge is estimated through the use of Empirical Formulation . Notably, the calibrated procedure is performed following the pre-fixed calibration and validation period.

Best-fit approach

In the case of empirical formulation, four potential distributions (linear, quadratic, power, and exponential) are selected as potential laws between Q and CM data as follows:

$$Q_{CM} = a\,(CM) + b \qquad \text{Eq.14a}$$

$$Q_{CM} = a\,(CM)^2 + b\,(CM) + c \qquad \text{Eq.14b}$$

$$Q_{CM} = a\,(CM)^b \qquad \text{Eq.14c}$$

$$Q_{CM} = a\,(b)^{CM} \qquad \text{Eq.14d}$$

CM and Q time series are, therefore, trained with the aforementioned formulations. To check the best-fit solution from the selected distribution, a model evaluation criterion has been set considering Akaike Information Criteria (AIC), Bayesian Information Criteria (BIC), and Pearson correlation coefficient (*r*). The best fit of any site has been obtained by lower values of AIC and BIC with a higher value of *r*; thus, a composite index (CI) is formulated to evaluate the overall model scores to determine the best-fit model for the selected site.

$$AIC = 2k - 2\ln L' \quad \text{Eq.15a}$$

$$BIC = k*\ln n - 2\ln L' \quad \text{Eq.15b}$$

$$CI = r + (1-AIC) + (1-BIC) \quad \text{Eq.15c}$$

where k equals to the number of parameters used in the model; n equals to the sample size, and L' is the maximum value of the likelihood function for the model.

6.4.2 Uncalibrated Approach

In the absence of coincident observations of Q and CM time series, the uncalibrated procedure uses the same framework proposed by Tourian et al. (2013). Here, the available discharge and retrieved CM signal time series are sorted independently in descending order. Subsequently, the corresponding exceeding probability of each value in the time series is computed for both Q and CM time series individually by considering their percentage of the observation periods. Here, for each site, the basic assumption is that the insitu Q and CM signals have the same exceedance probability. Developing the joint probability distribution by considering the individual cumulative distribution function (CDF) of Q and CM, the river discharge could be estimated from the standalone CM signals for any gauging sites. Thus, the CDF curves are calculated and compared to generate the percentiles associated with the discharges. With the relative correspondences between percentiles, it is possible to generate river discharge from the reflectance time series. Following this principle, the uncalibrated approach is performed along the selected gauging sites to estimate the long-term river discharge time series from the CM signals.

For generating long-term discharge time series using the CM signals, the calibrated procedure is based on the coincident observations of in situ Q and CM. The absence of CM signals during flood events due to the presence of cloud cover in the images may affect the model parameterization to capture the high flow dynamics both in Best Fit and Copula Fit solutions. Although the uncalibrated procedure is independent of the coincident observations of in situ Q and CM, the availability of the in situ Q data period is still a key concern. For instance, the hydrograph generated from a short event may not be representative of the long-term period; thus, derived CDF cannot find the proper solution while deriving the joint distribution, which also may add significant uncertainties while deriving long-term discharge time series. In both calibrated and uncalibrated procedures, there are possibilities to lose the flood information due to the unavailability of CM signals in the presence of cloud cover, which is very often too.

7 Derive discharge from merged products

The traditional process to estimate river discharge that uses data from altimetry is here advanced with the contribution of multispectral images and river width to overcome the limits of individual sensors related to the temporal frequency. The merging procedure is carried out through the L3 Merging approach.

Details on this approach will be provided in the next version of the document (v2.1).

8 References

Altenau, E. H., Pavelsky, T. M., Durand, M. T., Yang, X., Frasson, R. P. D. M., & Bendezu, L. (2021). The Surface Water and Ocean Topography (SWOT) Mission River Database (SWORD): A global river network for satellite data products. *Water Resources Research*, *57*(7), e2021WR030054. https://doi.org/10.1029/2021WR030054.

Andriambeloson, J. A., Paris, A., Calmant, S., & Rakotondraompiana, S. (2020). Re-initiating depth-discharge monitoring in small-sized ungauged watersheds by combining remote sensing and hydrological modelling: a case study in Madagascar. *Hydrological Sciences Journal*, *65*(16), 2709-2728.

Belloni, R., Camici, S., & Tarpanelli, A. (2021). Towards the continuous monitoring of the extreme events through satellite radar altimetry observations. *Journal of Hydrology*, *603*, 126870.

Biancamaria, S., Durand, M., Andreadis, K. M., Bates, P. D., Boone, A., Mognard, N. M., ... & Clark, E. A. (2011). Assimilation of virtual wide swath altimetry to improve Arctic river modeling. *Remote Sensing of Environment*, *115*(2), 373-381.

Bogning, S., Frappart, F., Paris, A., Blarel, F., Niño, F., Picart, S. S., ... & Braun, J. J. (2021). Hydro-climatology study of the Ogooué River basin using hydrological modeling and satellite altimetry. *Advances in Space Research*, *68*(2), 672-690.

Bogning, S., Frappart, F., Blarel, F., Niño, F., Mahé, G., Bricquet, J. P., ... & Braun, J. J. (2018). Monitoring water levels and discharges using radar altimetry in an ungauged river basin: The case of the Ogooué. *Remote Sensing*, *10*(2), 350.

Chow, V. T. (1959). *Open-Channel Hydraulics.* McGraw-Hill Education.

Chow, V. T., Maidment, D. R., & Mays, L. W. (1988). Applied Hydrology. McGraw-Hill Education. [Chapter 10: Open-Channel Flow, specifically sections discussing rating curves and power-law relationships]

Clayton, D. (1978) A model for association in bivariate life tables and its application in epidemiological studies of familial tendency in chronic disease incidence. *Biometrika* 65, 141–151. doi:10.1093/biomet/65.1.141

Elmi, O., Tourian, M. J., Bárdossy, A., & Sneeuw, N. (2021). Spaceborne river discharge from a nonparametric stochastic quantile mapping function. *Water Resources Research*, *57*(12), e2021WR030277.

Elmi, O., & Tourian, M. J. (2023). Retrieving time series of river water extent from global inland water data sets. *Journal of Hydrology*, *617*, 128880.

Elmi, O., Tourian, M. J., Saemian, P., and Sneeuw, N. (2024). Remote sensing-based extension of GRDC Discharge time series-a monthly product with uncertainty estimates. *Scientific Data*, *11*(1), 240. https://doi.org/10.1038/s41597-024-03078-6.

Filippucci P., Brocca L., Bonafoni S., Saltalippi C., Wagner W., Tarpanelli A. (2022) Sentinel-2 high-resolution data for river discharge monitoring. *Remote Sensing of Environment.*, 281, 113255, https://doi.org/10.1016/j.rse.2022.113255.

Filippucci, P., Sahoo, D. P., Tarpanelli A. (2025). Two decades of river discharge from multi-mission multispectral data, *Remote Sensing of Environment*, 329, 114919. https://doi.org/10.1016/j.rse.2025.114919.

Frank, M.J. (1979) On the simultaneous associative of f(x, y) and x + y − f (x, y). *Aequ. Math*. 19, 194–226 (1979). doi:10.1007/BF02189866 .

Frappart, F., Fatras, C., Mougin, E., Marieu, V., Diepkilé, A. T., Blarel, F., & Borderies, P. (2015). Radar altimetry backscattering signatures at Ka, Ku, C, and S bands over West Africa. *Physics and Chemistry of the Earth, Parts A/b/c*, *83*, 96-110.

Frasson R. P. D. M., Wei R., Durand M., Minear J. T., Domeneghetti A., Schumann G., Williams B.A., Rogriguez E., Picamilh C., Lion C., Pavelsky T. Garambois P.-A. (2017). Automated river reach definition strategies: Applications for the surface water and ocean topography mission. *Water Resources Research*, 53(10), 8164-8186.

Gelman, A., Carlin, J. B., Stern, H. S., Dunson, D. B., Vehtari, A., & Rubin, D. B. (2013). "Bayesian Data Analysis." Chapman and Hall/CRC.

Genest, C., Masiello, E., & Tribouley, K. (2009). Estimating copula densities through wavelets. *Insurance: Mathematics and Economics*, *44*(2), 170-181. https://doi.org/10.1016/j.insmatheco.2008.07.006.

Gilchrist, W. (2000). *Statistical modelling with quantile functions*. CRC Press.

Gumbel, E.J. (1960) Distributions des valeurs extrêmes en plusieurs dimensions. Publ. Inst. Stat. Univ. Paris 9, 171–173.

Hougaard, P. (1986) A class of multivariate failure time distributions. *Biometrika* 73, 671–678. doi:10.1093/biomet/73.3.671

Hoffman, M. D., & Gelman, A. (2014). "The No-U-Turn Sampler: Adaptively Setting Path Lengths in Hamiltonian Monte Carlo." Journal of Machine Learning Research, 15(1), 1593-1623

Kouraev, A. V., Zakharova, E. A., Samain, O., Mognard, N. M., & Cazenave, A. (2004). Ob'river discharge from TOPEX/Poseidon satellite altimetry (1992–2002). *Remote sensing of environment*, *93*(1-2), 238-245.

Liu, J., Bauer-Gottwein, P., Frias, M. C., Musaeus, A. F., Christoffersen, L., & Jiang, L. (2023). Stage-slopedischarge relationships upstream of river confluences revealed by satellite altimetry. Geophysical Research Letters, 50, e2023GL106394. https://doi.org/10.1029/2023GL106394.

McMahon, T. A., & Peel, M. C. (2019). Uncertainty in stage–discharge rating curves: application to Australian Hydrologic Reference Stations data. *Hydrological Sciences Journal*, *64*(3), 255-275.

Nash J.E., Sutcliffe J.V. (1970). River flow forecasting through conceptual models, part I—A discussion of principles. *Journal of hydrology*, 10(3), 282-290.

Neal J.C., Odoni N.A., Trigg M.A., Freer J.E., Garcia-Pintado J., Mason D.C., Wood M., Bates P. D. (2015). Efficient incorporation of channel cross-section geometry uncertainty into regional and global scale flood inundation models. *Journal of Hydrology*, 529, 169-183. https://doi.org/10.1016/j.jhydrol.2015.07.026

Papa, F., Bala, S. K., Pandey, R. K., Durand, F., Gopalakrishna, V. V., Rahman, A., & Rossow, W. B. (2012). Ganga-Brahmaputra river discharge from Jason-2 radar altimetry: an update to the long-term satellite-derived estimates of continental freshwater forcing flux into the Bay of Bengal. *Journal of Geophysical Research: Oceans*, *117*(C11).

Paris, A., Calmant, S., Gosset, M., Fleischmann, A. S., Conchy, T. S. X., Garambois, P. A., ... & Laraque, A. (2022). Monitoring Hydrological Variables from Remote Sensing and Modeling in the Congo River Basin. *Congo Basin Hydrology, Climate, and Biogeochemistry: A Foundation for the Future*, 339-366.

Paris, A., Dias de Paiva, R., Santos da Silva, J., Medeiros Moreira, D., Calmant, S., Garambois, P. A., ... & Seyler, F. (2016). Stage-discharge rating curves based on satellite altimetry and modeled discharge in the Amazon basin. *Water Resources Research*, *52*(5), 3787-3814.

Pekel, Jean-François; Cottam, Andrew; Gorelick, Noel; Belward, Alan (2017): Global Surface Water Explorer dataset. European Commission, Joint Research Centre (JRC) [Dataset] PID: http://data.europa.eu/89h/jrc-gswe-global-surface-water-explorer-v1 (last accessed 31 July 2025)

Rantz, S. E. (1982). *Measurement and computation of streamflow* (Vol. 2175). US Department of the Interior, Geological Survey.

Robert, C. P., & Casella, G. (2004). "Monte Carlo Statistical Methods." Springer.

Saemian, P., Elmi, O., Stroud, M., Riggs, R., Kitambo, B. M., Papa, F., Allen, G.H. and Tourian, M. J. (2024). Satellite Altimetry-based Extension of global-scale in situ river discharge Measurements (SAEM). *Earth System Science Data Discussions*, *2024*, 1-29. https://doi.org/10.5194/essd-17-2063-2025.

Sahoo, D.P., Sahoo, B., and Tiwari, M.K. 2020. Copula-based probabilistic spectral algorithms for high-frequent streamflow estimation. *Remote Sensing of Environment*, 251, 112092.

Tarpanelli A., Brocca L., Lacava T., Melone F., Moramarco T., Faruolo M., Pergola N., Tramutoli V. (2013) Toward the estimation of river discharge variations using MODIS data in ungauged basins. *Remote Sensing of Environment*, 136, 47–55. https://doi.org/10.1016/j.rse.2013.04.010.

Tarpanelli A., Brocca L., Barbetta S., Faruolo M., Lacava T., Moramarco T. (2015) Coupling MODIS and radar altimetry data for discharge estimation in poorly gauged river basin. *IEEE Journal of Selected Topics in Applied Earth Observations and Remote Sensing*, 8(1), 141-148. https://doi.org/10.1109/JSTARS.2014.2320582.

Tourian, M. J., Schwatke, C., & Sneeuw, N. (2017). River discharge estimation at daily resolution from satellite altimetry over an entire river basin. *Journal of Hydrology*, *546*, 230-247.

Tourian, M. J., Sneeuw, N., & Bárdossy, A. (2013). A quantile function approach to discharge estimation from satellite altimetry (ENVISAT). *Water Resources Research*, *49*(7), 4174-4186.

Vörösmarty, CJ et al. (1998): Discharge compilation from The Global River Discharge (RivDIS) Project. Distributed Active Archive Center, Oak Ridge National Laboratory, PANGAEA, https://doi.org/10.1594/PANGAEA.859439.

Zakharova, E., Nielsen, K., Kamenev, G., & Kouraev, A. (2020). River discharge estimation from radar altimetry: Assessment of satellite performance, river scales and methods. *Journal of Hydrology*, *583*, 124561.

Zakharova E., S Agafonova, C Duguay, N Frolova, A Kouraev. (2021). River ice phenology and thickness from satellite altimetry: potential for ice bridge road operation and climate studies. The Cryosphere, 15 (12), 5387-5407.